3.2.3.2 Estimating earthquake displacement of the cliff crest

There are no reliable monitoring data that covers exactly the period of the 2010/11 Canterbury earthquakes. However, it is possible to estimate the likely magnitude of the displacement of the main cracked areas at the cliff crest during the 22 February and 13 June 2011 earthquakes, by subtracting the cumulative inferred displacements from crack apertures as follows:

Total displacement inferred from the mapping of crack apertures over the period corresponding to the two main earthquakes was about 0.2–1.9 m, adopting only those displacements from cracks with measurements of both horizontal and vertical displacements, and recorded along cross-sections 1–6 (Table 6).

Field mapping of the cliff crest was again carried out by Geotech Ltd. following the 13 June 2011 earthquake. This mapping measured pre-existing cracks and any new cracks that may have formed in response to these earthquakes (Appendix 5). These displacements are summarised for each cross-section in Table 7.

Permanent slope displacement of the cliff crest along the cross-sections can be estimated by subtracting the 13 June 2011 earthquake displacements (Table 7) from the total displacements (Table 6), to derive a range of possible displacements that may have occurred during the 22 February 2011 earthquakes. These magnitudes are inherently uncertain (Table 8).

Permanent slope displacement of the cliff crest during the 16 April and 23 December 2011 earthquakes are unknown. Site observations suggest little reactivation of existing cracks with only a few new cracks appearing (Appendix 5).

Table 7 Measured cumulate crack apertures, horizontal only, which formed during the 13 June 2011 earthquakes, measured by M. Yetton (Geotech Ltd.; Appendix 4). Displacements are inferred from field mapping of tension crack apertures along survey lines. Errors are nominally estimated as being ±0.01 m (values are rounded to the nearest 10 mm).

Cross-section	Source Area	Vertical component (mm)	Horizontal component (mm)
1 and 4	1	Not measured	230–610
2 and 5	2	Not measured	180–200
6	3	Not measured	650–680

Table 8 Inferred cumulative crack apertures for the 22 February 2011 earthquakes. Calculated by subtracting the inferred displacements in Table 7 from the inferred total displacements in Table 6, along corresponding cross-sections.

Cross-section	Source Area	Vertical component (mm)	Horizontal component (mm)
1 and 4	(Source area 1)	750–1430	330–1320
2 and 5	(Source area 2)	370	10–280
6	(source area 3)	880	230–260

3.2.3.3 Surveyed slope displacements

The survey monitoring data are presented in Appendix 4 and summarised below. There are two data sets:

1. Cadastral survey marks (details held by Land Information New Zealand) i.e., property boundaries and roads footpaths etc.; and
2. Monitoring survey marks installed by Aurecon NZ Ltd., for Christchurch City Council, to monitor surface displacement.

Both datasets adopt reference control marks outside the area of landslide movement, but still within the local area. Therefore, regional offsets caused by the tectonic displacements are largely removed from the data.

Cadastral marks (source: LINZ)

Available cadastral survey marks were resurveyed by GNS Science to detect absolute ground movements spanning the earthquake period from before the 22 February 2011 earthquakes (the pre-earthquake survey dates for each cadastral mark vary) to 11 February 2012, and therefore include total displacements of the survey marks in response to the earthquakes within this time period. Only two survey marks are located in the cracked areas behind the slope crest (cadastral survey marks 35 and 42, Appendix 4 Map 2), and therefore do not represent the overall movement of the slope.

The results of this survey are contained in Appendix 4 (Map 2). Vector displacements indicate permanent ground displacements in the order of about 0.2–0.3 m. These are thought to represent lower-bound estimates of the total displacement during the earthquakes, at the cliff crest, as these survey marks were located outside the main areas of cracking.

Monitoring marks (source: Aurecon NZ Ltd.)

The displacements calculated using the Aurecon survey data span the time period 5 November 2012 to 5 April 2013 and there are approximately five observations per mark. Note that the dates covered and the numbers of observations vary per survey mark. The marks are installed only in assessed source areas 2 and 3, and no marks are installed in assessed source area 1.

These data do not span the time frame corresponding to the 2010/11 Canterbury earthquakes. From the survey time series relating to each mark it has been possible to determine the magnitudes and bearings of any displacement over the monitoring period. The only displacements calculated from the monitoring marks that are larger than the associated error (monitoring mark ID's5 and 17, Map 3, Appendix 4), were:

- Mark 5: 12 mm/year towards bearing 350–355°; and
- Mark 12: 12 mm/year towards bearing 280–290°.

The displacement of monitoring mark 5 is consistent with the field-measured displacement (of 30 mm towards the north) of "tell-tale" survey pegs installed by Geotech Ltd., indicating displacement occurred sometime between November 2012 and April 2013.

The displacement of monitoring mark 17 is consistent with the area of extension and compression at the cliff crest immediately west of assessed source area 2. This movement is not thought to relate to displacement of the rock slope, as the direction of movement is away from the steeper slope. This displacement is inferred to be related to displacement of the mapped slump.

3.2.3.4 Volumes of debris lost from the cliffs

Changes of the cliffs in response to the 2011 earthquakes have been quantified using repeat terrestrial laser scan surveys and LiDAR surveys (Table 9) with field mapping.

Table 9 Estimated volumes lost from the cliffs calculated from the terrestrial laser scan (TLS) and LiDAR surveys.

Change model	Volume leaving slope (m^3)	Area of slope face (m^2)[3]	Volume loss per unit area (m^3/m^2)	Probable trigger
Estimate by PHGG consultants after the 4 September 2010 earthquake	60 (±10)	22,000	0.003	4 September 2010 earthquake (M_w 7.2)
Airborne LiDAR: 2003–March 2011 (2011a)[1]	23,800 (±6600)	22,000	1.08	22 February 2011 earthquake (M_w 6.2)
TLS: 6 March 2011–3 May 2011[2]	1,170 (±110)	22,970	0.05	16 April 2011 earthquake (M_L 5.6)
Airborne LiDAR: March 2011–July 2011[1]	11,800 (±3500)	22,970	0.51	13 June 2011 earthquake (M_w 6.2)
TLS: 16 June 2011–16 January 2011[2]	1,180 (±130)	22,870	0.05	23 December 2011 earthquake (M_w 6.1)
TLS: 16 January 2011–19 December 2012[2]	440 (±160)	22,870	0.02	No obvious trigger possible rainfall induced
TLS: 19 December 2012–12 November 2013	81 (±47)	22,870	0.004	No obvious trigger possible rainfall induced

[1] Change models derived from airborne LiDAR surveys carried out by AMM Hatch (2003) and New Zealand Aerial Mapping (2011a, March 2011 and 2011c, July 2011); refer to Appendix 2 for details.

[2] Change models derived from terrestrial laser scan surveys carried out by GNS Science, refer to Appendix 3 for details.

[3] Slope surface areas are estimated for each change model using the LiDAR slope surface at the time of the earthquake, and the area where changes to the slope face occurred.

Digital elevation models representing the ground surface at a given time were generated for each data set. For the LiDAR surveys, a 1 m grid (ground resolution) of elevations was generated from filtered scan data points supplied by the contractor. For each of the terrestrial laser scan surveys a 0.1 m grid was generated from the filtered point data. Filtering comprised removal of points representing vegetation and buildings from the supplied point data, thereby creating a "bare earth" or "filtered" point elevation data set. This was undertaken by GNS Science for the terrestrial laser scan survey data, and by the consultants AAM Hatch and New Zealand Aerial Mapping for the LiDAR datasets (these companies were commissioned by other parties, mainly the Earthquake Commission and the Christchurch City Council, to carry out the surveys).

Errors are assessed for each digital elevation model by comparing the modelled surface with the filtered point data used to generate it. Errors in the terrestrial laser scan survey data are generally ±0.05–0.09 m at one standard deviation and for the LiDAR data generally ±0.1–0.3 m (in height) for the New Zealand Aerial Mapping data sets (LiDAR surveys 2011a and 2011c), and ±0.3–0.5 m (in height) for the AAM Hatch data sets.

3.2.4 Subsurface movement

Drillhole inclinometer tubes were used to monitor displacements at depth, assess whether movement was occurring along single or multiple slide-surfaces, and to independently verify the results of surface monitoring. Monitoring is undertaken manually by commercial contract (Geotechnics Ltd.).

Inclinometer tubes were installed in drillholes BH-MB-01, BH-MB-02 (Pletz and Revell, 2013), and BH-GDV-01 (Tonkin and Taylor, 2012a). The inclinometer displacements are monitored at 0.5 m intervals and the inclinometer accuracy is quoted as ±6 mm over 25 m of tubing (Slope Indicator, 2005). The measurement details are summarised in Table 10.

The inclinometers installed in drillholes BH-MB-01 and BH-MB-02 show no movement of the inclinometer tubes greater than the associated error, and therefore indicate no displacement. However, the inclinometer tube installed in BH-GDV-01 has a deflection between the 2.25 and 3.25 m (below the collar elevation) intervals. The deflection is relatively small, about 2 mm in the A-Axis plot, and is marginally outside the associated error. The monitoring reports received do not indicate what bearing of movement this is towards. The deflection is only recorded in one survey, it is not known if there are more recent survey records.

The deflection occurred between the 25 October 2011 and 24 December 2011 inclinometer surveys (Tonkin and Taylor, 2012a), and corresponds to the base of the loess/volcanic colluvium logged in the drillhole, suggesting displacement along rockhead. This displacement may be related to the 23 December 2011 earthquake. Any deeper-seated displacement of the underlying rock mass forming the cliff would not have been measured by the inclinometer, as the inclinometer base is only 10 m below ground level, compared to a cliff height (cliff crest to toe) of about 70 m.

Table 10 Summary of drillhole inclinometer surveys.

Measuring date	Drillhole ID		
	BH-MB-01[1]	BH-MB-02[1]	BH-GDV-01 (Tonkin and Taylor, 2012a)
15/07/2011	N/A	N/A	Base reading
8/09/2011	N/A	N/A	No movement outside error
16/09/2011	N/A	N/A	No movement outside error
12/10/2011	N/A	N/A	No movement outside error
25/10/2011	N/A	N/A	No movement outside error
24/12/2011			About 2 mm in cumulative displacement plot at a depth interval between 2.25 and 3.25 below ground level.
4/04/2013	Base reading	Base reading	No data
5/06/2013	No movement outside error	No movement outside error	No data
21/03/2014	No movement outside error	No movement outside error	No data

[1] Geotechnics Ltd Report 720085.000/RPT (Geotechnics, 2014).

3.2.5 Groundwater

Drill water circulation conditions reported in drilling records (Pletz and Revell, 2013) indicate water losses occurred in drillholes BH-MB-01 and BH-MB02, and were in the range from 10 to 100% (percentage of water flush lost into the ground), but generally between 80 and 100%. BH-MB-01 was reported as being dry by the driller (no water return). Groundwater levels in the Tonkin and Taylor (2012a) drillhole BH-GDV-01 were 0.6–1.8 m below ground level, and ground water was not encountered in CPT-GDV-01 and CPT-GDV-02.

There are three standpipes installed in the assessment area. These were installed by Tonkin and Taylor Ltd in drillhole BH-GDV-01 and cone penetration holes CPT-GDV-01 and CPT-GDV-02. The bottom of the standpipe response zones are reported to be in loess, at depths of between 2.8 m and 3.5 m below ground level.

Monitoring data from the standpipes comprise the manual measurement of water levels in the standpipes. Approximately 3–14 measurements were made over the reporting period 3 August 2011–29 May 2012 (Tonkin and Taylor, 2012a), indicating a poor temporal resolution. No more recent data are available to GNS Science at the time of writing this report. The data show that standpipes CPT-GDV-01 and CPT-GDV-02 were dry at the times they were measured. Measurements from standpipe BH-GDV-01 show water levels in the loess at around 1 m below ground level, with the bottom of the response zone being at about 2.3 m below ground level, for the period 8 August 2011 to about 11 November 2011. The reading made around 9 April 2012 indicated that the standpipe was dry.

It is possible that groundwater is present in the other standpipes, but that the poor temporal resolution has not allowed them to be resolved. Springs and water seepage have been noted (Figure 11). There are also reports of increased storm water flow over the cliff edge due to damaged services.

These data suggest there is some groundwater present at the site but that it is probably confined within the loess at the cliff crest. It should be noted that standpipe BH-GDV-01 is downslope and within about 10 m of a main storm water drain, which appears to be broken. Drilling records indicate that the rock mass, forming the steep rock slope, is predominantly dry with no permanent water table apparent, and that during drilling, circulation of drilling fluids was lost, indicating a highly permeable rock mass.

3.3 ENGINEERING GEOLOGICAL MODEL

An engineering geological map is presented in Figure 11, site investigation map in Figure 12 and cross-sections 1–6 in Figure 13. The map and cross-sections are based on the interpretation of features identified in aerial photographs, field mapping and ground investigation data.

3.3.1 Slope materials

3.3.1.1 Fill

Localised areas of fill relating to the construction of residential homes can be found over much of the site. The depth and extent of these localised areas are unknown, although the inferred boundaries of the fill are shown on cross-sections in Figure 13 (where mapped). The fill, where encountered in drillholes, is described as soft and relatively weak silt with occasional clasts of basalt and concrete. The thickness of the fill, unless encountered in drillholes, is unknown, but it is estimated to be up to several metres in places.

3.3.1.2 Talus

The talus at the toe of the cliff – present before the 2010/11 Canterbury earthquake-induced talus accumulations – comprises several car-sized boulders along with many smaller boulders of volcanic rock that have fallen from the cliff. Much of this material has slaked – due to wetting and drying cycles – indicating that the original rockfall volumes were probably larger than the volume of talus currently present.

The recent accumulations of talus and boulders triggered by the 2010/11 Canterbury earthquakes are shown on Figure 11. Site observations – post-2010/11 earthquakes – indicate that these volcanic materials are already slaking. Sampling for particle size distributions of the talus has not been carried out for health and safety reasons. However, estimates made from photographs and terrestrial laser scan surveys, suggest the majority of the debris comprises boulders of diameter greater than 0.5 m.

3.3.1.3 Loess

The loess mantling the slope within the assessment area is similar to other areas of the Port Hills. It is a relatively cohesive silt-dominated soil with only minor clay mineral content. Its strength is largely controlled by the soil moisture content and this has been well studied, e.g., Bell et al. (1986), Bell and Trangmar (1987), McDowell (1989), Goldwater, (1990), Yetton (1992) and Carey et al. (2014). In some places the loess appears to have been reworked by construction activities for the residential dwellings.

The loess in the main zone of cracking at the cliff crest is unsaturated and relatively strong where exposed. Similarly, the thin layer of loess/volcanic colluvium sometimes present above the bedrock and at the base of the loess does not appear particularly weak or wet. The loess

is highly hydroscopic and when exposed to water (rain) it quickly disintegrates into muddy silt. The thickness of the loess mantling the cliff top inferred from drillhole and trial pit records and from field mapping of exposures, varies between less than 1 m and up to 3 m, but up to 4 m well back from the cliff edge.

3.3.1.4 Colluvium

A layer, of sandy silt containing boulders and gravel with minor clay was logged in drillholes BH-GDV-01, BH-GDV-02, BH-BAL-01, BH-MB-01 and BH-MB-02. Codd and Revell (2013) describe this material as highly variable and dominated by either silts or gravel and cobbles. The thickness of the colluvium varies from about one metre near the cliff crest to less than 0.3 m and less further back from the cliff crest.

Given that all drillholes encountered this material, it has been assumed that volcanic colluvium mantles rockhead and underlies the loess over most of the site. Where exposed in outcrop, the colluvium appears to have slightly higher clay content than those materials described in the drillhole logs. It is thought to represent the deposits of debris from past landslides and other erosion processes. The material derives mainly from weathered volcanic breccia and lava and remobilised loess. In drillholes and field exposures, the colluvium is highly variable. It ranges from gravel to boulder-sized clasts of volcanic basalt with a loess and clay matrix, to remoulded loess with occasional gravel and boulders.

3.3.1.5 Bedrock (volcanic basalt lava breccia and lava)

The cliff face comprises gently dipping (and locally steeply dipping) interlayered variations of four main rock types – in order from the cliff crest to cliff toe: 1) an upper basalt lava breccia that appears generally massive, interlayered with discontinuous and thin blocky columnar-jointed basalt lava flows; 2) blocky columnar-jointed basalt lava flow that is highly variable in thickness (from 10 m to less than 1 m and in some areas is missing completely); 3) epiclastic layer within the basalt-breccia/lava sequence ranging from coarse, poorly sorted conglomerates and sandstones, to tuffaceous clays and silts and rare but prominent palaeosols; and 4) a lower basalt lava breccia that is generally massive and interlayered with discontinuous and thin blocky columnar-jointed basalt lava flows.

The material layering is highly variable both laterally and vertically but the layers are laterally persistent along most of the cliff. Descriptions of the main units are given in Table 11 and shown in Figure 14.

The general dip/dip direction of the volcanic sequence in the north of the site is dip of 10–15° towards dip direction 290–320°, which is well constrained by the rock exposures in the cliff face along Nayland Street (Massey et al., 2012a). This dip becomes less to the south, where it is essentially horizontal and some areas appear to dip out of the slope. However, there are significant variations within the sequences. In the central part of the cliff the trachy basalt lavas form a steeply-inclined dome (possible lava dome) locally dipping into the slope at about 60°.

Discontinuity data derived from photogrammetric surveys of the Redcliffs cliffs and kinematic assessment of the various discontinuity-controlled failure modes is contained in Appendix 10.

Table 11 Engineering geological descriptions of the main geological units forming the cliffs (descriptions as per New Zealand Geotechnical Society, 2005).

Unit name	Description
Basaltic lava breccia	Slightly weathered to highly weathered, light grey to dark grey when slightly weathered to orange or red-brown when highly weathered, massive, brecciated basaltic lava fragments, moderately strong to strong (but varies to weak or very weak when highly or completely weathered), with very widely spaced irregular discontinuities. At all sites basaltic lavas have flowed within thick carapaces of brecciated lava, with the breccia often exceeding the thickness of its source lava (brecciated units may be 2 to >10 m thick.). Breccias are poorly graded, angular lava fragments with a fine to coarse matrix supporting unsorted cobbles, blocks and often 1–5 m diameter megablocks of broken lava. Breccia fragments are often more vesicular and scoriaceous than the source lava, and prone to weathering due to high porosity. Bedding is massive, poorly jointed, with lower boundaries gradational with the source lava and upper boundaries roughly planar. Weathering expression is cavernous and spheroidal, of fine and coarse blocks respectively, and in some cases development of cliff parallel exfoliation joints/cracks. Freshly exposed breccia faces show extensive interstitial clay weathering and deposition of clay within vesicles and between clasts. Most joints are due to recent fracturing of the rock mass during the 2010/11 earthquakes, with very little tectonic discontinuities, if any, apparent. Joints are very widely spaced (>2 m), with their persistence varying from a few metres to tens of metres. Joint surfaces tend to be "fair" to "good" adopting the Geological Strength Index classification (Hoek, 1999).
Basalt lava	Dark greenish grey to black, unweathered to moderately weathered, sometimes vesicular, Basalt, very strong with variably developed columnar joints, widely to very widely spaced (1.5–5 m), typically giving large to very large block sizes that are columnar in shape. Columnar joints are often radial to flow margins, and lavas have gradational contacts with lava breccia at their upper and side margins. Joint faces are generally rough to very rough, stepped or irregular, commonly manganese oxide or calcite coated, and only rarely have clay or silt fill. Joint surfaces therefore tend to be "fair" to "good" adopting the Geological Strength Index classification (Hoek, 1999). Individual flows form lensoidal bodies throughout the cliffs, ranging from 0.5 to 2–4 m thick. Columnar jointing is well expressed where flows are thick, and gives way to thin, platy flow orientated jointing where flows are thin.
Epiclastic deposits	Moderately to highly weathered or oxidised brown to red-brown or yellow-brown thinly bedded Tuff or Tuffaceous Sandstone, intercalated with or grading into fine to coarse pebbly Lapilli Tuffs or gravelly sandstone and conglomerate, with occasional cobble-sized blocks and bombs of basalt, moderately strong to weak, very weak to extremely weak when highly weathered. Rarely jointed, prone to cracking on exposed surfaces and easily eroded. Bedding is thin (0.1–2 m) and discontinuous, disrupted by overlying lavas. In all sites, these layers of red-oxidised pyroclastic and epiclastic paleosol material are found between lava flows and breccias, usually at the top of the preceding lava breccia, and oxidised/baked by the overlying lava flow. The thinly bedded ash and lapilli, with occasional blocks and bombs, is discontinuous due to re-working by water-driven epiclastic processes or re-working by overlying lava flows. The pyroclastic material exposed in the cliffs is often vegetated or a focus for fluid flow, being relatively impermeable compared to the overlying jointed lavas and porous breccias. Contacts are often gradational into lava breccia or lahar/debris-flow deposits.

Figure 14 View to the west onto the main cliff at Redcliffs. (**A**) is basalt lava breccia, (**B**) is columnar jointed basalt lava and breccia (**C**) is the epiclastic layer that generally forms a recessive slope, and the material below this is basalt lava breccia (**D**). Photograph by C. Gibbons (July 2011). For surveyed boundaries between materials refer to Appendix 3.

3.3.2 Geotechnical properties

Material strength parameters have been assigned based on the results from in-house (GNS Science) laboratory tests and the published results of testing of similar materials from elsewhere in the Port Hills.

3.3.2.1 Loess and colluvium

Material parameters adopted for the loess and loess derived colluvium material in the assessment area are shown in Table 12. These are based on: 1) descriptions of the drillcore materials; and 2) Port Hills soil strength test results reported by Carey et al. (2014) and others.

Table 12 Range of adopted bulk soil strength parameters for Redcliffs soils.

Soil Unit	Unit weight (kN/m^3)	Intact Young's modulus E_i (MPa)	Poisson's ratio	Cohesion c (kPa)	Friction ϕ (°)	Tensile strength (kPa)
Loess and loess derived colluvium	17	30	0.3	10	30	10

3.3.2.2 Volcanic bedrock

In order to derive rock mass strength parameters for the volcanic breccia, lava and epiclastic that take into account the nature of the discontinuities as well as the intact strength of the material, the Geological Strength Index (Hoek, 1999) was adopted using Rocscience RocLab software.

The Geological Strength Index values adopted for the main materials are shown in Figure 15. Strength tests of Redcliffs rock samples from drillholes BH-MB-01 and BH-MB-02 are shown in Table 13, and are taken from Carey et al. (2014). Mohr-coulomb parameters (cohesion and friction) were derived from Rocscience RocLab software by line fitting over the appropriate stress range of the slope.

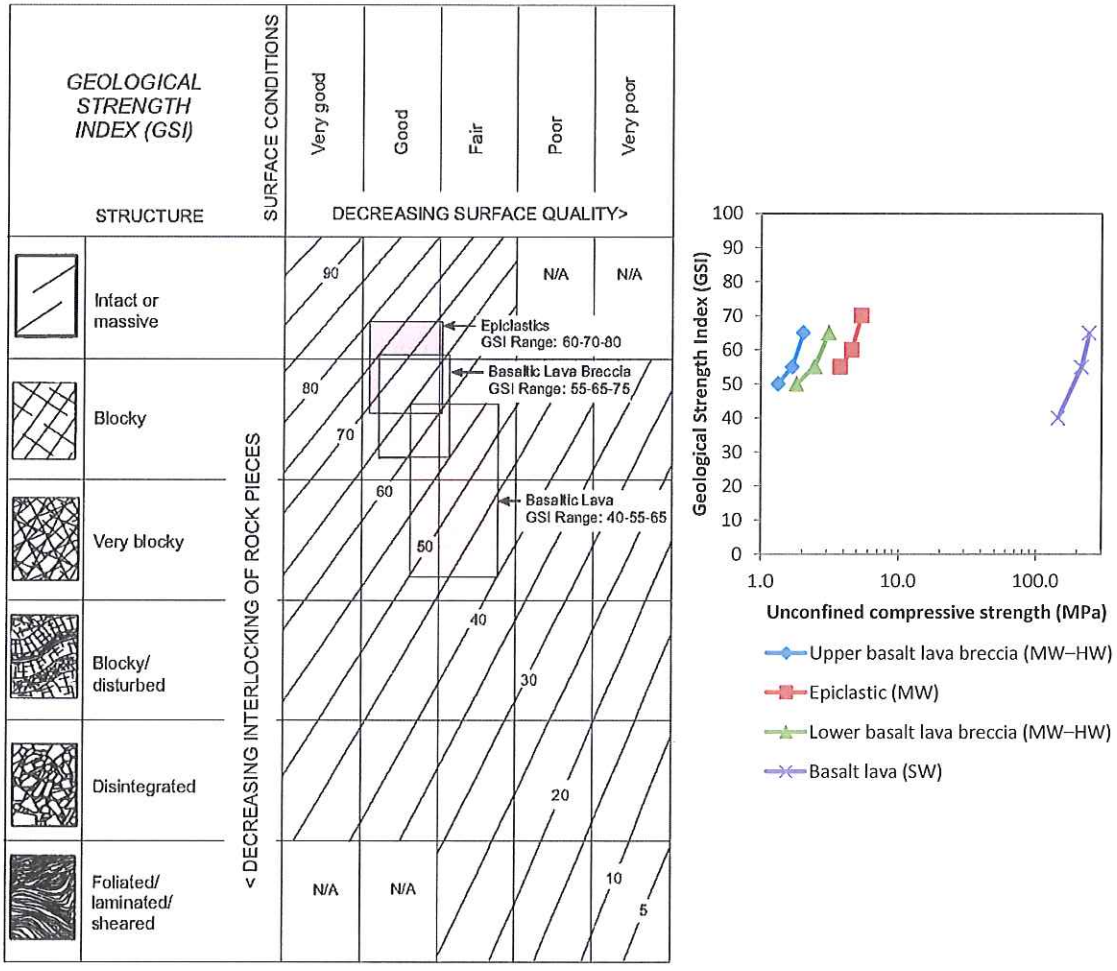

Figure 15 Geological Strength Index plot for volcanic breccia and lava at Redcliffs (modified after Hoek 1999). B) The adopted lower, middle and upper estimates of GSI per given material type plotted against the corresponding lower middle and upper unconfined compressive strength from the laboratory testing (Table 12).

Results from laboratory testing (Carey et al., 2014) show that the upper breccia is weaker than the lower breccia, and that the strength of the breccia is related to its moisture content. The laboratory test results indicate that the samples from the upper breccia had higher moisture contents and lower unconfined compressive strengths to those tested samples from the lower breccia.

Table 13 Range of adopted rock strength parameters (for cross-section 4).

Unit	Range[1]	Laboratory test results						Rock mass parameters derived from RocLab							
		Bulk unit weight (kN/m^3)	Unconfined compressive strength (MPa)	Tensile strength (MPa)	Tangent modulus of deformation (MPa)	m_i[2]	Poisson's ratio	Average Slope Height above unit (m)	GSI[1]	Lithostatic stress range (kPa)	Sampling stress tangent (kPa)	Cohesion[3] c (kPa)	Friction[3] ϕ (°)	Tensile strength (kPa)	Modulus E_M (MPa)
Upper basalt lava breccia	MAX	18.4	2.0	0.4	770	5.0	0.18	30	65	0–540	270	100	31	21	380
	AVG	18.2	1.7	0.3	600	5.6	0.13		55			70	23	11	180
	MIN	18.0	1.3	0.2	430	6.9	0.07		50			64	21	8	132
Basalt lava	MAX	28.0	243	14.7	54,700	16.5	No data, assumed 0.2	30	65	0–540	270	3,100	68	730	13,080
	AVG	28.0	214	11.8	38,800	18.1			55			1,650	69	340	8,450
	MIN	27.0	146	10.6	21,200	13.8			40			670	68	129	3,380
Epiclastic	MAX	19.5	5.4	0.6	1,710	9.5	0.1	30	70	0–540	270	190	47	50	880
	AVG	18.9	4.55	0.48	1,180	9.5	0.10		60			130	38	36	330
	MIN	18.2	3.7	0.4	640	9.4	0.1		55			120	37	20	260
Lower basalt lava breccia	MAX	19.5	3.1	0.5	1,550	5.7	0.4	70	65	540–1,260	900	250	26	26	880
	AVG	18.8	2.5	0.4	1,390	6.1	0.3		55			160	14	22	500
	MIN	18.0	1.8	0.3	1,230	7.0	0.2		50			146	13	15	380

1 MIN, AVG and MAX represent the range (minimum, average, maximum) of test results and field measurements.

2 The m_i values shown, represent the range in the ratio of unconfined compressive strength to tensile strength, derived from tested samples of basalt lavas and basalt lava breccias (Carey et al., 2014), and not the ratio of unconfined compressive strength to tensile values shown in the table.

3 Mohr-coulomb parameters (cohesion and friction) were derived from RocLab by line fitting over the appropriate stress range of the slope.